Bioorganic Chemistry 85 (2019) 140–151

Contents lists available at ScienceDirect

Bioorganic Chemistry

journal homepage: www.elsevier.com/locate/bioorg

3, 9-di-O-substituted coumestrols incorporating basic amine side chains act as novel apoptosis inducers with improved pharmacological selectivity

Guoshun Luo[a,b,1], Zhengpu Tang[a,b,1], Xinyu Li[a,b], Qiangqiang Hou[a,b], Yu Chen[b,c], Kejing Lao[d], Hua Xiang[a,b,*]

[a] State Key Laboratory of Natural Medicines, Jiangsu Key Laboratory of Drug Design and Optimization, China Pharmaceutical University, Nanjing 210009, China
[b] Department of Medicinal Chemistry, School of Pharmacy, China Pharmaceutical University, Nanjing 210009, China
[c] Key Laboratory of Smart Drug Delivery, Ministry of Education School of Pharmacy, Fudan University, Lane 826, Zhangheng Road, Shanghai 201203, China
[d] Shaanxi Key Laboratory of Brain Disorders and Institute of Basic and Translational Medicine, Xi'an Medical University, Xi'an, Shaanxi 710021, China

ARTICLE INFO

Keywords:
Coumestrol
Estrogenic activity
Apoptosis
Cell cycle
Tubulin polymerization inhibitor

ABSTRACT

There is much interest in the use of phytoestrogens such as coumestrol in breast cancer intervention due to their antiestrogenic activity and multiple modes of tumor cell death. However, the clear beneficial effects of naturally occurring estrogen mimetic coumestrol remain controversial due to experimental evidence that it has been shown to stimulate MCF-7 cell proliferation via agonist effect on estrogen receptor at low concentration. Herein, to disconnect the ER interaction and apoptosis-specific mechanism of coumestrol, various 3, 9-di-O-substituted coumestrols (**7a**-**7e**) and their furan ring-opened analogs (**5a**-**5e**) were synthesized and assessed for antiproliferative properties. Attachment of a dimethylamine-containing side chain to 3-O of coumestrol led to the most promising compound **7e** with improved antiproliferative activity (1.7-fold increase) against MCF-7 cells, decreased estrogen activity (> 20 times weaker ERα binder) and a novel action to induce apoptosis. Mechanistic studies revealed that **7e** is a tubulin polymerization inhibitor, which could arrest cell cycle at G2/M phase and induce apoptosis along with the decrease of mitochondrial membrane potential. In summary, such subtle modifications to the 3, 9-di-hydroxyl groups of coumestrol allow the generation of a novel apoptosis inducer with distinct pharmacological properties, providing an excellent starting point to future development of novel tumor-vascular disrupting agents targeting tubulin.

1. Introduction

With their diverse structures and bioactivity, natural products historically have been a rich source of lead compounds for drug development. Of the drugs approved by the US Food and Drug Administration (FDA), > 40% of them developed over the past 30 years are from NP or their structural scaffolds [1,2]. For anticancer drugs, over 60% of these drugs approved since 1940 can be traced to a natural product [3]. Discovery and development of anticancer agents from plants have shown promise for cancer prevention and therapeutics. As part of our recent research to develop new anti-cancer agents, we were attracted to the coumarin-based derivatives [4,5], which are common components of biologically active natural products [6].

Coumestan (6H-[1]benzofuro[3,2-*c*]chromen-6-one) is an important class of phytochemicals containing a planar and oxygenated tetracyclic scaffold in which one coumarin ring is fused with a benzofuran ring (Fig. 1). Natural coumestans are widely distributed in a variety of plant species belonging to botanical families such as *Fabaceae*, *Leguminosae* and *Asteraceae* [7] and exhibites various biological activities such as antioxidative [8], antitubercular [9], and antineoplastic effects [10], depending on their diverse structures modified by substituents on the ring system. Coumestrol (Fig. 1) is a representative member in the coumestan family and was first identified as a phytoestrogen with estrogenic properties by E. M. Bickoff in ladino clover and alfalfa in 1957 [11]. It has garnered great research interest stemming from its antiestrogenic activity and prevalence in many human diets, including

Abbreviations: ER, estrogen receptor; E2, estradiol; 2-ME2, 2-methoxyestradiol; MOA, mode of action; MTT, 3-(4,5-dimethylthiazol-2-yl)-2,5-diphenyltetrazolium bromide; JC-1, 5,5′,6,6′-tetrachloro-1,1′,3,3′-tetraethyl-benzimidazolcarbocyanine; MMP, mitochondrial membrane potential

* Corresponding author at: State Key Laboratory of Natural Medicines, Jiangsu Key Laboratory of Drug Design and Optimization, China Pharmaceutical University, Nanjing 210009, China.
E-mail address: xianghua@cpu.edu.cn (H. Xiang).

[1] Same contribution to this paper.

https://doi.org/10.1016/j.bioorg.2018.12.024
Received 22 August 2018; Received in revised form 7 November 2018; Accepted 18 December 2018
Available online 22 December 2018
0045-2068/

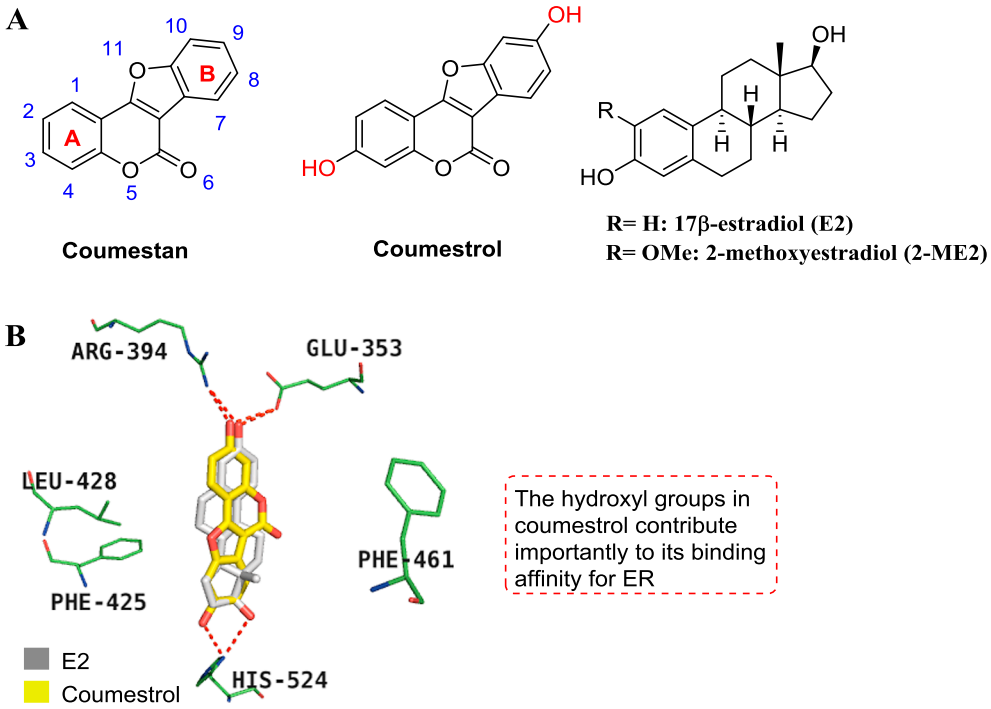

Fig. 1. (A) Chemical structures of coumestan, coumestrol, endogenous estrogen (17β-estradiol, E2) and estradiol metabolite 2-ME2. (B) ERα LBD complexes showing the ligand-binding orientations of coumestrol compared to E2 (PDB: 3UUD).

soybeans, brussels sprouts, spinach and a variety of legumes [12]. These two hydroxy groups of coumestrol orients in the same position as those in the endogenous estradiol (E2) (Fig. 1), allowing it to disrupt the activity of estrogen receptor (ER), which highlighted the potential of coumestrol as a therapeutic approach targeting hormone-dependent breast cancer. However, the role of phytoestrogens like coumestrol in treating breast cancer remains contradictory and elusive. Several analyses that assessed soy exposure and breast cancer risk revealed that the chemoprotective effects of phytoestrogens are dependent on early exposure and high soy consumption [13–16]. There is evidence that at low pharmacologic concentrations, coumestrol produces negative effects, such as inducing further growth of existing breast cancer tumors by activating ERα receptors [17–19].

Recently, prof. Jordan VC and colleagues have investigated this matter and concluded that phytoestrogens may be used as an effective treatment for breast cancer due to their apoptotic properties [20]. When it comes to its apoptotic activity, coumestrol was also reported to exhibit broad-spectrum anti-proliferative effects [21–23] through a variety of mechanisms which involve increasing ROS generation and modulation of cell cycle progression in breast and colon cancer [24–26], stimulating mitochondria-mediated intrinsic apoptosis in breast and prostate cancer cells [27,28] and regulating PI3K and MAPK signal transduction cascades in prostate and ovarian cancer cells [29].

Concerns regarding the effects of coumestrol on promoting cell growth and proliferation in ER positive breast tumors have been linked to its agonistic activity on ERα leading to upregulation of gene expression similar to estrogen [30,31]. From known phytoestrogen activities, it has been shown that mimicking the phenolic function of estrogen is most important for ERα binding and thus is the most likely pharmacophore in coumestrol [32,33]. Indeed, analysis of the X-ray crystal structure of coumestrol on ERα reveals that the phenolic hydroxyl groups of coumestrol form a tight network of hydrogen bonds with the key residues Glu353, Arg394 and His-524 in human ERα (Fig. 1B), which are similar to that of E2 within human ERα [34]. This specific binding pattern of phenolic groups of estrogen and coumestrol within ERα is encouraging to the prospects that proper modification of dihydroxy in coumestrol allowing for a general blocking of access to the phenolic function might be an alternative strategy to undermine its ERα agonistic activity [35], while amplifying and enhancing mechanisms of apoptosis.

Inspired by the wide range of antiproliferative activities and relatively simple structure-activity relationship (SAR) of coumestrol, we report herein the design and screening of a series of 3, 9-di-O-substituted coumestrols and their furan ring-opened analogs as specific apoptosis inducers (Fig. 2) [36]. A set of hydrophilic amines that are widely accepted in clinical approved drugs were introduced to 3-OH position of coumestrol which would also help to improve the drug likeness of natural coumestrol with high molecular rigidity. The *in vitro* antiproliferation screening against both ER-positive breast cancer cells (MCF-7) as well as other two solid tumor cells (PC3 and HepG2) identified compound **7e** as the most promising apoptosis inducer that showed lower ERα binding effect. Further mechanism study demonstrated that **7e** can induce apoptosis, reduce mitochondrial transmembrane potential, and arrest the cell cycle at the G2/M phase in MCF-7 cells via tubulin polymerization inhibition.

2. Results and discussion

2.1. Chemistry

Various synthetic approaches have been reported to facilitate the construction of tetracyclic scaffold of coumestans due to the diversie pharmacological activities [37–40]. Among these, the $FeCl_3$-mediated direct intramolecular oxidative annulation of 4-hydroxy-3-arylcoumarins that can efficiently lead to diversified coumestan derivatives was relatively more concise and straightforward [41,42]. This method was successfully applied to the synthesis of key intermediate 9-O-methylcoumestrol (**6**) by using a protection-deprotection protocol in 5 steps with 18% overall yield [42]. To improve the overall yield, here we reported a more efficient route which involves Friedel-Crafts acylation, diethyl carbonate (DEC) mediated in situ lactonization and $FeCl_3$-mediated intramolecular cyclization (Fig. 3). Notably, compound **6** is prepared in fewer steps (3 steps) with higher overall yield (35%) than prior approach and protecting group is not required.

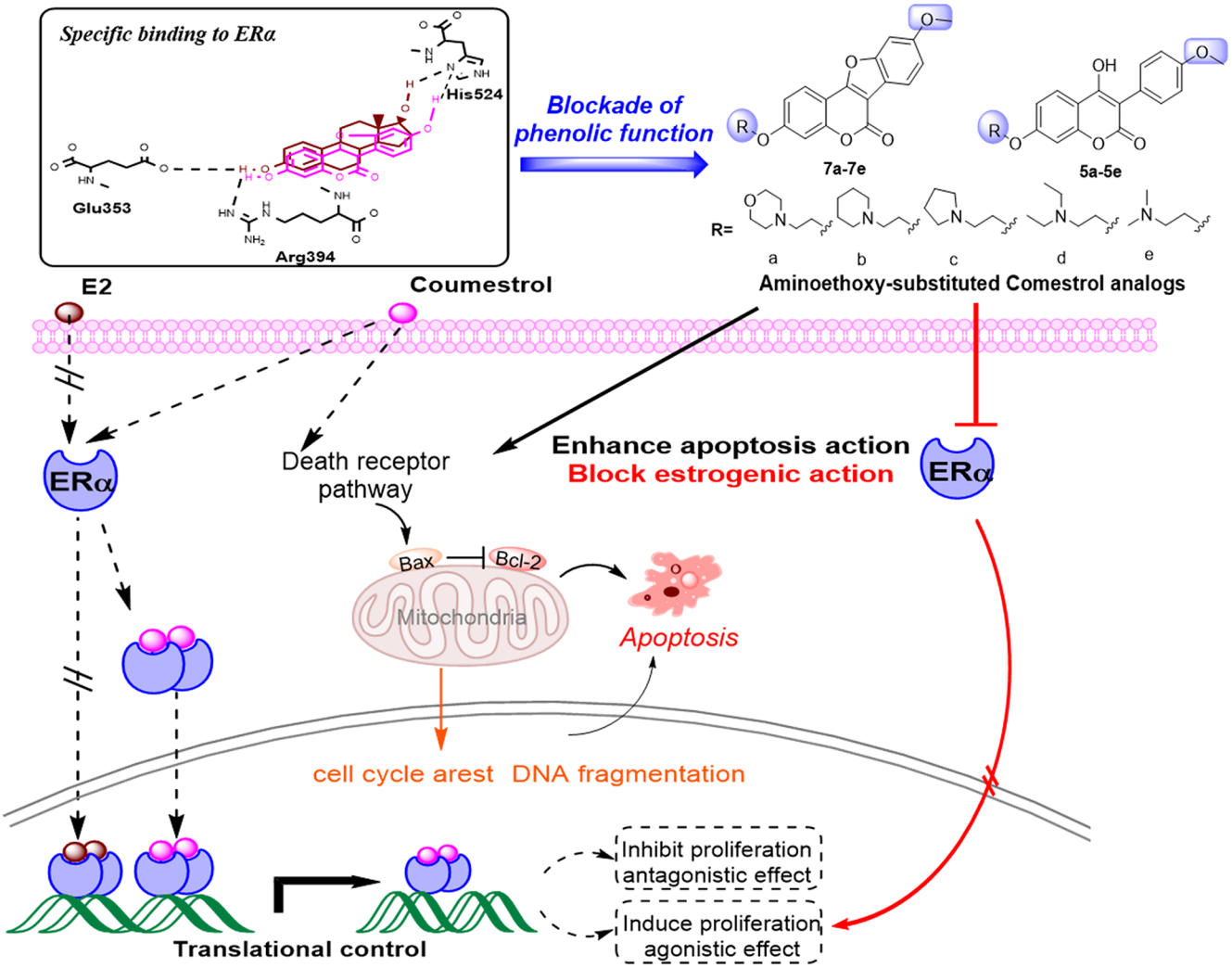

Fig. 2. A schematic diagram illustrating the current working hypothesis regarding improved pharmacological selectivity induced by aminoethoxy-substituted comestrols selectively targeting apoptosis pathways in breast cancer cells. (Upper left) Binding results of E2 and coumestrol within ERα. (Upper right) Design of the aminoethoxy-substituted comestrols as pure apoptosis inducers. (Lower) Signaling pathway in dashed lines indicates the paradox of coumestrol-induced breast cancer cell growth and apoptosis; signaling pathway in bold lines indicates the proposed mechanisms of apoptosis induced by our newly designed coumestrol analogs that are expected to be lack of ERα agonistic activity.

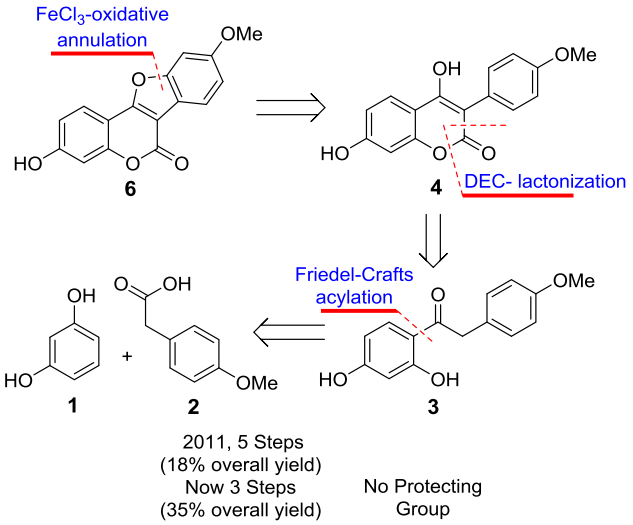

Fig. 3. Retrosynthetic analysis of key intermediate 9-O-methylcoumestrol (**6**).

The general preparation methods for target compounds **5a**-**5e** and **7a**-**7e** are displayed in Scheme 1. Firstly, commercially available resorcinol (**1**) and 4-hydroxybenzoic acid (**2**) were treated with BF_3-Et_2O to yield benzophenone (**3**) in 76% yield. Further treatment of compound **3** with diethyl carbonate (DEC)/NaH in reflux toluene gave 3-aryl-4-hydroxyl coumarin (4) with yield 75%, which were then converted to the final compounds **5a**-**5e** by regioselectively substituted with corresponding 2-chloro-1-amine hydrochloride. On the other hand, compound **4** underwent FeCl**3**-mediated oxidative cyclization to give the intermediate 9-O-methylcoumestrol (**6**) in 61% yield. Finally, the desired 3, 9-di-O-substituted coumestrols **7a**-**7e** were achieved via a nucleophilic substitution in good yields.

2.2. Biological evaluation

2.2.1. In vitro antiproliferative activity

All the newly synthesized compounds **5a**-**5e** and **7a**-**7e** obtained with acceptable log P (logarithm of the octanol/water partition coefficient) values (3.7 < ClogP < 5.2) were first evaluated for their antiproliferative activities against four human cancer cell lines: MCF-7 (human breast cancer), PC3 (human prostate cancer), HepG2 (human

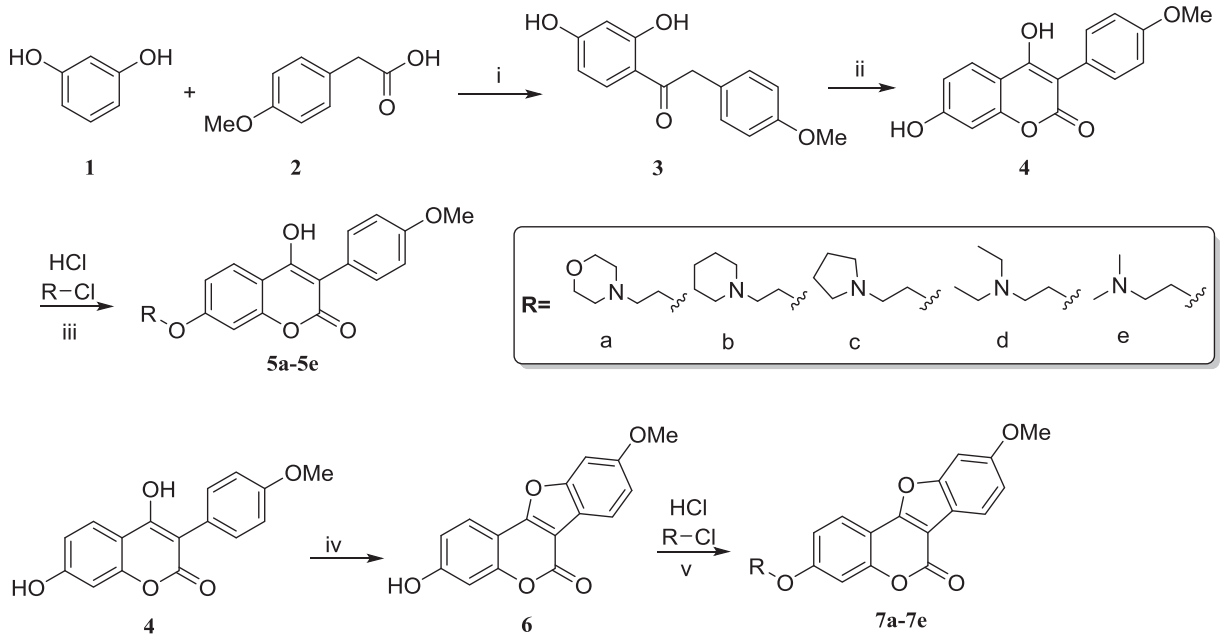

Scheme 1. Synthetic routes of 5a–5e and 7a–7e. Reagents and conditions: (i) BF_3-OEt_2, 80 °C, 1.5 h, 76%; (ii) NaH, DEC, anhydrous toluene, 120 °C, 2 h, 75%; (iii) Na_3PO_4, various 2-chloro-amine hydrochlorides a-e, anhydrous DMF, 90 °C, 5–7 h; (iv) anhydrous $FeCl_3$, SiO_2, DEC, reflux, 5 h, 61%; (v) Na_3PO_4, various 2-chloro-amine hydrochlorides a-e, THF, 60 °C, 4–7 h.

Table 1
Structures, antiproliferation activity and physical-chemical properties of compounds **5a-5e** and **7a-7e**.

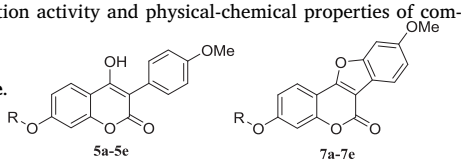

Cmpd	R	Antiproliferation (IC_{50}, μM)[a]				cLogP[b]
		MCF-7	PC3	HepG2	HCT116	
5a		> 80	> 80	> 80	> 80	3.7
5b		55.3	68.2	61.7	58.7	4.9
5c		> 80	> 80	> 80	> 80	4.4
5d		> 80	> 80	> 80	> 80	4.8
5e		> 80	> 80	> 80	> 80	3.7
7a		58.5	> 80	> 80	> 80	4.0
7b		> 80	69.5	73.2	> 80	5.2
7c		42.1	46.2	42.9	39.3	4.6
7d		52.2	45.3	62.8	51.4	5.0
7e		27.8	30.2	35.1	34.6	3.9
coumestrol	–	46.7	45.6	58.5	49.2	3.1
5-Fu	–	27.4	26.7	37.3	34.3	–

[a] IC_{50}: concentration that inhibits 50% of cell growth after 72 h of treatment. The IC_{50} values are expressed as mean values of experiments performed in triplicate.

[b] ClogP values were calculated by ChemBioDraw Ultra 14.0.

liver cancer) and HCT116 (human colon cancer) by using a conventional MTT (3-(4,5-dimethylthiazol-2-yl)-2,5-diphenyl tetrazolium bromide) assay. Lead compound coumestrol and the clinically used drug 5-fluorouracil (5-Fu) were used as positive compounds for comparison. Initially single-dose screening (80 μM) was carried out to evaluate the inhibitory activity of each compound. The IC_{50} values of those active compounds in the single-dose cytotoxicity tests at 80 μM (Inhibition% > 50%), are listed in Table 1. It was found that coumestrol and 5-Fu showed moderate growth inhibition of MCF-7, PC3 HepG2 and HCT116 cancer cells with IC_{50} values of 46.7–58.5 and 27.8–35.1 μM, respectively, which is highly comparable to the reported data [26,29,43]. As a global observation, the 3, 9-di-O-substituted coumestrol analogs (**7a-7e**) were preferable for cancer cell growth inhibition compared with the corresponding furan-ring opened analogs (**5a-5e**) most of which were inactive against the three cancer cells with IC_{50} values more than 80 μM. Furthermore, analysis of the influence of different basic group on antiproliferative activity suggested a preference for three small size basic group, dimethylamine, and diethylamine and pyrrolidinyl (**7c**, **7d** and **7e**) which exhibited comparable or better antiproliferative activity than positive controls. Especially, analogue **7e** bearing a dimethylamine moiety was much potent than the parent compound coumestrol against MCF-7, PC3 HepG2 and HCT116 cancer cells with IC_{50} values of 27.8, 30.2 35.1 and 38.6 μM, respectively.

Among the tested coumestrol analogues, analogue **7e** exhibited the most active anticancer activity on MCF-7, PC3, HepG2 and HCT116 cancer cells compared to others and displayed an approximately 1.5-1.7-fold increase in potency comparted with lead compound coumestrol. Additionally, the results of *in silico* ADME studies indicated that **7e** exhibited good physicochemical characters along with non-violation of Lipinski's rule of five (Table S1). Therefore, **7e** was selected for the following pharmacological studies on the most sensitive MCF-7 cells.

2.2.2. Estrogen receptor competitive binding assay and cell viability assay

Several in vitro studies showed that many phytoestrogens including coumetrol actually stimulate ERα-positive breast cancer cell proliferation at low concentration (< 1 μM) [44–46]. This undesirable response is likely due to the agonistic effect through ERα activation at low concentration [31]. To determine the influence such substitution of coumestrol had on the interaction with ERα, we employmed a Polar Screen™ ERα competitor assay kit to compare the binding affinity of **7e** and coumestrol at ERα. The assay used fluorescence polarization to monitor displacement of a fluorescently tagged estrogen (Fluromone TM Tracer) from the ERα/Fluromone TM Tracer complex. The

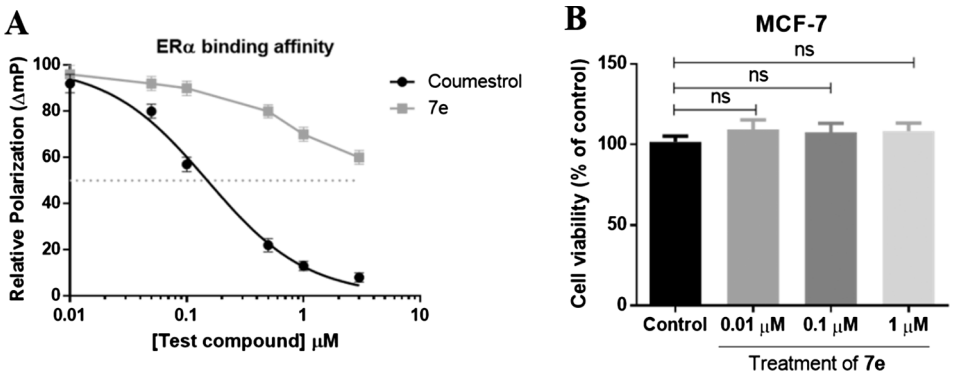

Fig. 4. (A) ERα binding affinity of 7e and coumestrol. 7e (IC_{50} > 3) proved to be at least 20 times weaker binder than coumestrol (IC_{50} = 0.15). (B) MCF-7 cell viability over 72 h exposure to 0.01–1 μM 7e. No significant stimulation of cell proliferation was observed after treatment of 7e.

polarization value remains high when the Fluromone TM Tracer is bound to the estrogen receptor, while the compounds displaced the Fluromone TM Tracer cause a low polarization value. As is shown in Fig. 4A, coumestrol exhibited strong ERα binding affinity even at low concentration of 0.1 μM and displaced 50% of the fluorescently tagged estrogen at 0.15 μM. Gratifyingly, our dimethylamine containing coumestrol derivative **7e** showed no/negligible affinity rate at less than 1 μM concentrations and proved to be at least 20 times weaker binder than this parent coumestrol.

Coumestrol as well as E2 were reported to exhibit estrogenic activity by stimulating MCF-7 cell proliferation, reaching 2–4 times more than control cells at low concentrations (0.01–1 μM) [46]. To further test the estrogenic activity of **7e**, its effect on proliferation of the ERα-positive breast cancer cell line (MCF-7) at low concentration (0.01–1 μM) was assessed. As expected, our compound **7e** did not induce proliferation at any of the doses tested (Fig. 4B). All these results suggested that **7e** has improved mechanism selectivity while lacking the undesirable estrogen properties associated with tumor cell production especially at low concentration, which showed that substitution to both sides of the phenols is required to see drastic changes in ERα binding interactions.

2.2.3. Analogue *7e* induced MCF-7 cell apoptosis and G2/M cell cycle arrest

Apoptosis induction or cell cycle arrest or combined effects are considered to be effective cancer therapeutic methods [47]. Therefore, to gain further evidence relating the growth inhibition induced by **7e** in MCF-7 cells, an annexin V-FITC/propidium iodide (PI) binding assay was performed. The cells were treated with **7e** at indicated concentrations (0, 10, 15 and 20 μM), then analyzed by flow cytometry. As shown in Fig. 5, treatment of **7e** for 24 h increased both early and late apoptotic ratios from 5.18% of vehicle control to 13.21% (10 μM), 28.20% (15 μM) and 38.50% (20 μM) in a concentration-dependent manner. Indicating that **7e** was an effective apoptosis inducer.

Similarly, effect of **7e** on cell cycle arrest in MCF-7 cells was investigated by a flow cytometry analysis using PI staining. The results showed that treatment of **7e** (0, 10, 15 and 20 μM) obviously resulted in accumulation of MCF-7 cells in G2/M phase in a dose-dependent manner (Fig. 5).

2.2.4. Analogue *7e* induced mitochondrial dysfunction

Mitochondrial changes, including loss of mitochondrial membrane potential (MMP), are key events that take place during drug-induced apoptosis [48]. To further investigate the effect of **7e** on mitochondrial function, quantitative MMP assay using JC-1 staining was performed in MCF-7 cells. As shown in Fig. 6, various concentrations of **7e** significantly increased the number of JC-1 monomers (green fluorescence intensity) and decreased that of JC-1 aggregates (red fluorescence intensity). Taken together, **7e** could induce MMP collapse and mitochondrial dysfunction in a dose-dependent manner, which eventually triggers apoptotic cell death.

2.2.5. Effect of analogue 7e on expressions of Cdc2, Bcl-2 and Bcl-xl

It is known that the activation of Cdc2 kinase could regulate eukaryotic cell entry into mitosis, leading to the cell division [49]. Thus, the association between **7e**-induced G2/M arrest and the alterations of protein Cdc2 expression was investigated by western blot analysis. As shown in Fig. 8A, after MCF-7 cells were treated with **7e** at the concentrations of 10 and 15 μM for 24 h, the expression of Cdc2 protein distinctly decreased in dose-dependent manner. Additionally, western blot analysis was also performed to investigate the effect of **7e** on mitochondrion-initiated apoptosis proteins (eg. bcl-2 and Bcl-xl). Results in Fig. 7(B and C) indicate that levels of anti-apoptotic protein Bcl-xl and Bcl-2 decreased in MCF-7 cells after expolsure of **7e** (10 and 15 μM). This result further confirmed that **7e** induced mitochondrial dysfunction and the mitochondrial pathway is involved in **7e**-induced apoptosis in MCF-7 cells.

2.2.6. Discovery of tubulin polymerization inhibition as the MOA for *7e*

According to the preliminary in vitro biological results, compound **7e** could be promising anticancer lead that exhibited improved pharmacological selectivity compared with the parent coumestrol (Fig. 8). However, to further design compounds with better drug-like properties and pharmacological activity based on this scaffold, it is necessary to identify a specific protein as the potential target for **7e**. The broad range of tumor cell lines in which compound **7e** showed acceptable growth inhibition together with its low ERα binding affinity suggested that a mode of action (MOA) in addition to ERα inhibition may be involved for this compound. This suppose is supported by the mechanism of an estradiol metabolite 2-ME2 (Fig. 1A), which shows 500-fold lower ERα binding affinity than estradiol while possessing anticancer and anti-angiogenesis activities through microtubule disruption and pro-apoptotic pathways [50,51]. Moreover, like most tubulin destabilizing agents, **7e** showed significant effect on the G2/M cell cycle arrest, hence it was considered of interest to investigate the tubulin polymerization aspect [52].

Inspired by above findings, we performed the tubulin assembly assay in a cell-free system to examine whether the compound **7e** interact with tubulin and inhibit tubulin polymerization in vitro. The well-known tubulin polymerization inhibitor colchicine and parent coumestrol were employed as controls. As shown in Fig. 9A, at 10 μM, **7e** induced improved inhibition of tubulin polymerization compared with coumestrol control. Simultaneously, it is worth noting that **7e** (inhibition rate of 75.5%) showed a closely tubulin inhibitory potency to the positive control colchicine (82.7%). Later, IC_{50} against tubulin polymerization was determined for compound **7e**, where it showed IC_{50} of 7.4 μM. Moreover, the furan ring-opened analogue **5b** revealed no

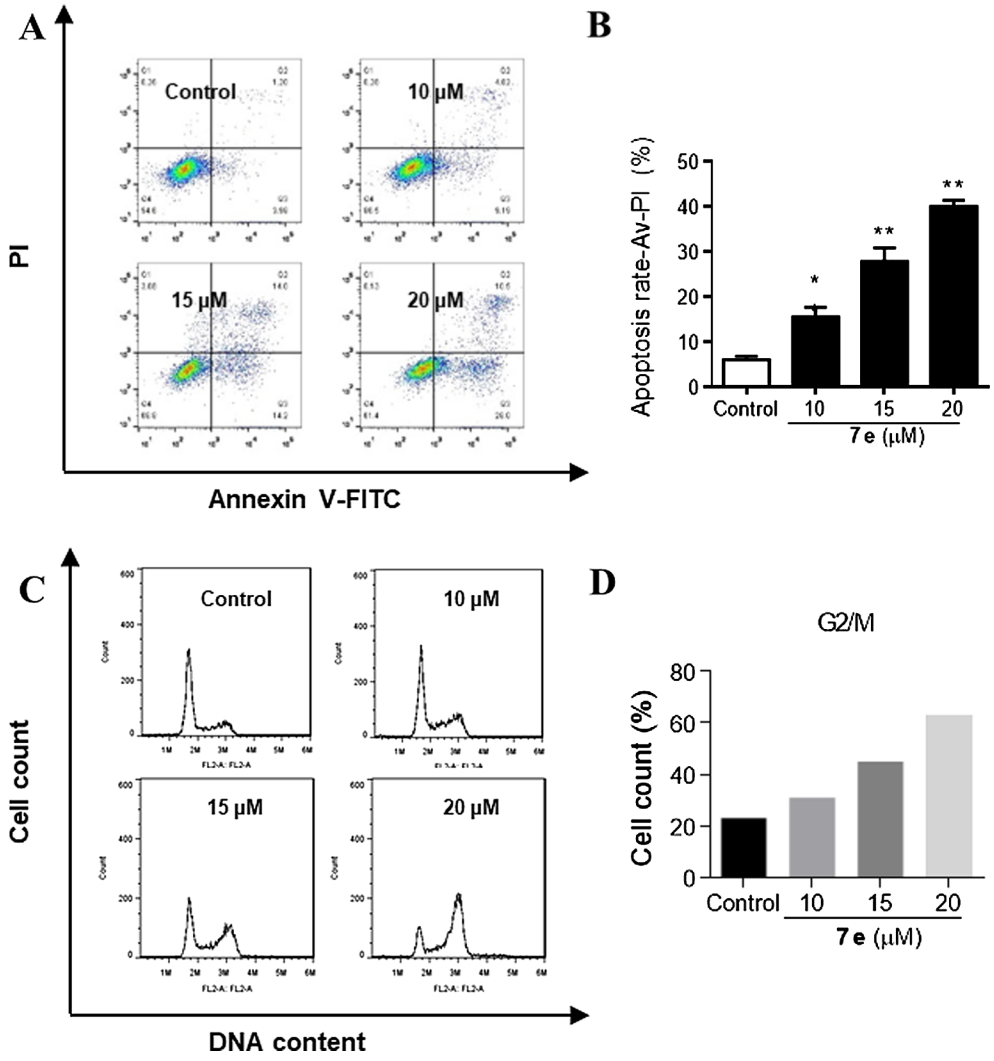

Fig. 5. (A) Flow cytometric apoptosis staining analysis of MCF-7 cells after 24 h treatment with 7e (10, 15, 20 μM) and no treatment (DMSO): viable (lower left), early apoptotic (lower right), late apoptotic (upper right), and necrotic cells (upper left). (B) The proportion of early and late apoptotic cells. Values are mean ± SD (n = 3). *P < 0.05, **P < 0.01 vs. Control group. (C) Cell cycle distribution of MCF-7 cells treated with 7e (0, 10, 15 and 20 μM) and no treatment (DMSO) for 24 h. (D) The proportion of MCF-7 cells in G2/M phase.

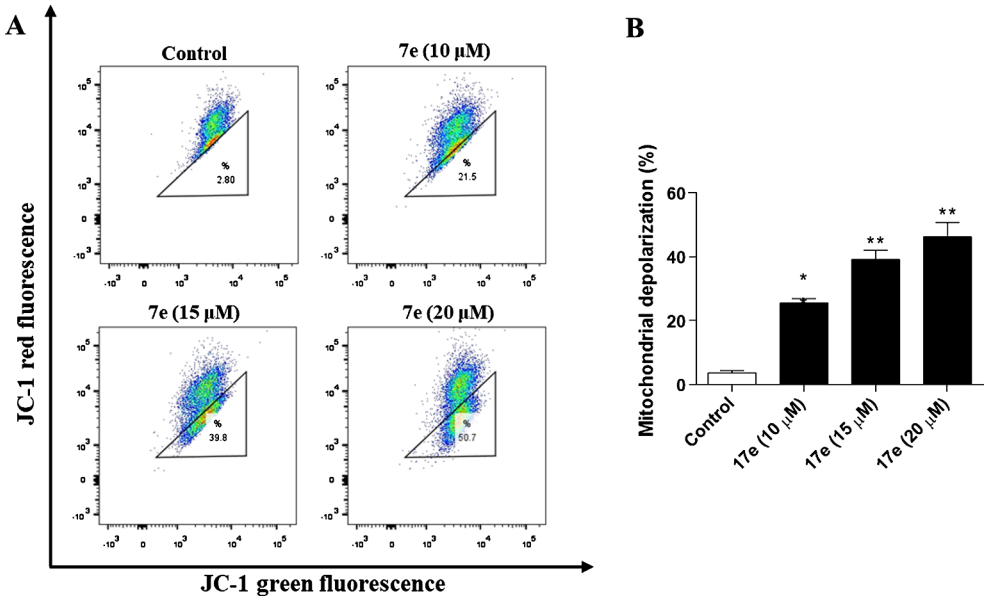

Fig. 6. (A) Compound 7e decreased the mitochondrial membrane potential in a dose-dependent manner. The MCF-7 cells were treated with 7e at the indicated concentration (10, 15, and 20 μM) or DMSO (0.01%) for 24 h, followed by incubation with the fluorescence probe JC-1 for 30 min. Then, the cells were analyzed by flow cytometry. (B) Values are mean ± SD (n = 3). *P < 0.05, **P < 0.01 vs. Control group.

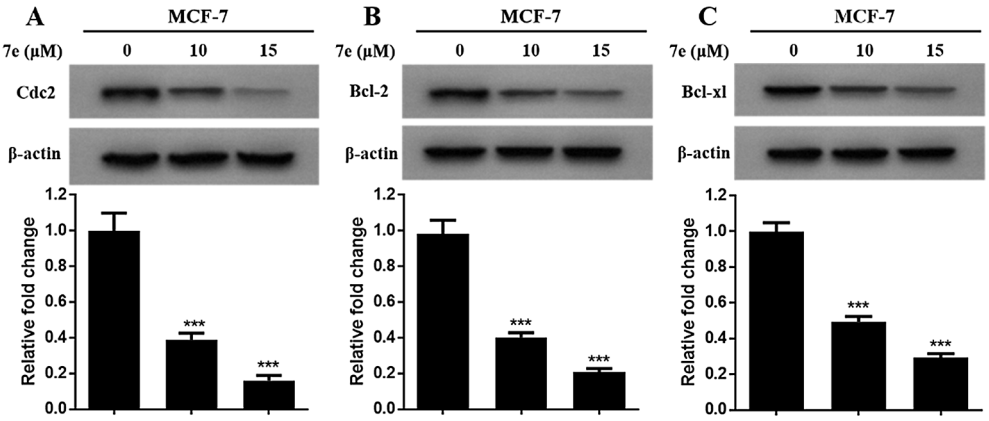

Fig. 7. The expression of proteins Cdc2 (A), Bcl-2 (B), and Bcl-xl (C) were analyzed by the western blot. Values are mean ± SD (n = 3). *P < 0.05, **P < 0.01, ***P < 0.001 vs. Control group.

significant influence on tubulin assembly, which is consistent with its poor cytotoxicity observed in Table 1. An excellent correlation was observed between the antiproliferative activity and inhibition of tubulin polymerization for **7e**, indicating that the molecular target of **7e** is most likely tubulin.

To determine the direct effects of compound **7e** on the disruption of microtubule dynamics in the living cells, we further exploymed immunofluorescence techniques to investigate alterations in the microtubule network in MCF-7 with colchicine as the positive control. As given in Fig. 9B, the microtubule network in untreated control cells displayed normal arrangement and organization. Whereas treatment with compound **7e** at less than IC_{50} concentration of 15 μM for 24 h led to disrupted microtubule network in MCF-7 cells. Similar pattern was observed when the cells were treated with colchicine (at concentration of 1 μM). These data suggested that **7e** acts as a mitotic inhibitor by blocking cell cycle progression through directly disrupting spindle assembly.

2.2.7. *In vivo anti-angiogenic activity of 7e*

It has been described that tubulin binding agents exhibit in addition to its antimitotic properties also important vascular disrupting activity targeting pre-existing tumor vasculature [53]. Chick embryo chorioallantoic membrane (CAM) is a highly vascularized structure, usually utilized to study angiogenesis and antiangiogenic compounds *in vivo* [54]. Towards this purpose, compound **7e** (3, 10 and 30 μM) dissolved in DMSO were placed on sterile methyl cellulose filter papers with phosphate buffered saline (PBS) as the blank control and 2-ME2 (3 and 10 μM) as the positive control. As shown in Fig. 10, compound **7e** effectively inhibited angiogenesis in a dose-dependent manner compared with PBS-treatment group where a massive production of newly formed blood vessels was observed. And compound **7e** exhibited similar inhibitory potency as that of 2-ME2 in CAM assay at the same dose, suggesting a promising *in vivo* anti-angiogenesis effect of **7e**.

3. Discussion

There has been much interest in the use of phytoestrogens in breast cancer prevention due to some epidemiological evidence of an inverse association between soy consumption in Asian countries and decreased breast cancer risk [13,14,55]. Coumestrol, a major representative of biphenolic phytoestrogen family, has been investigated as a possible substitute for hormone therapy and chemotherapy in breast cancer patients. However, the clear beneficial effects of these estrogens remain controversial [15], for example, researchers cannot clearly define phytoestrogens like coumestrol as being chemoprotective agents or potentially having negative effects, such as inducing further growth of existing breast cancer tumors by activating ERα receptor [17,20]. Current efforts are evaluating the mechanisms of coumestrol-induced apoptosis and how this new biology can be amplified and enhanced, thereby increasing the value of this therapeutic opportunity for the treatment of breast cancer [20]. To the best of our knowledge, there is no study relating the attempt of designing novel coumestrol analogues possessing decreased estrogenic activity and enhanced apoptosis in medicinal chemistry aspect. Encouragingly, the specific binding mode in which 3, 9-dihydroxyl groups of coumestrol form a tight network of hydrogen bonds with key residues in ERα hopefully provides the prospect that proper blockade of access to the phenolic function of the coumestrol scaffold should allow for a disconnection of estrogenic activity and apoptosis. To improve the therapeutic index of naturally occurring phytoestrogen coumestrol, the present study explored the

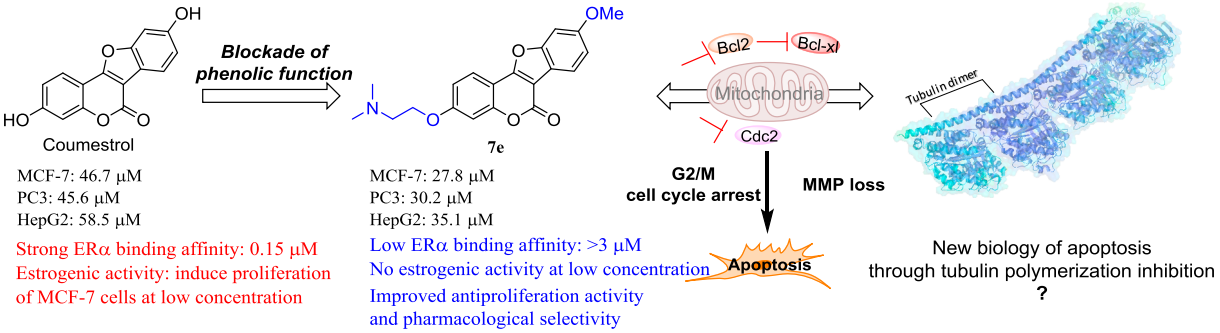

Fig. 8. Schematic diagram shown the promising activity of 7e compared with coumestrol and the proposed tubulin-targeted pathway for 7e-induced apoptosis in MCF-7 cells.

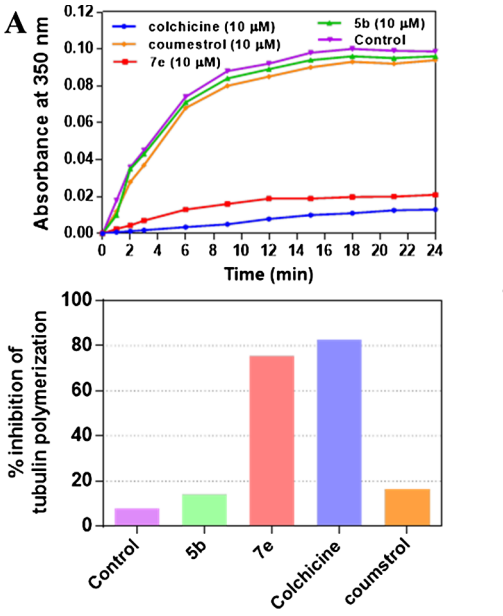

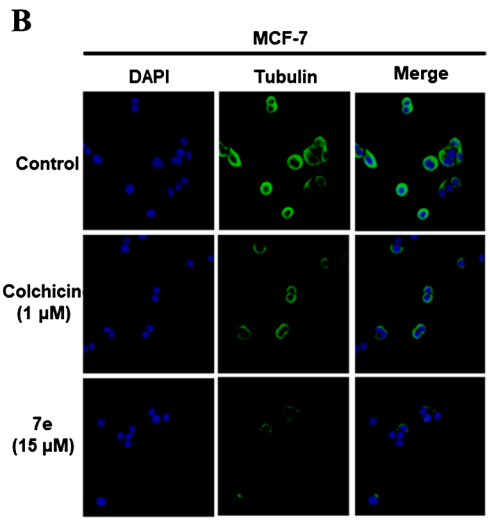

Fig. 9. (A) Purified porcine microtubules were incubated at 37 °C in the absence DMSO control or presence of drugs (colchicine, coumestrol or compounds 5b and 7e at concentration of 10 μM). Absorbance at 350 nm was measured every 3 min for 24 min and is presented as the increased polymerized microtubule. Final tubulin polymerization rate (control %) at 24 min was calculated by increase in the fluorescence mentioned above at 37 °C. (B) Effects of 7e on the cellular microtubule networks visualized by immunofluorescence: MCF-7 cells were independently treated with 7e at 15 μM and colchicine at 1 μM concentration for 24 h. Following the termination of the experiment, cells were fixed and stained for tubulin. DAPI was used as the counter stain and the merged images of cells stained for tubulin and DAPI are seen.

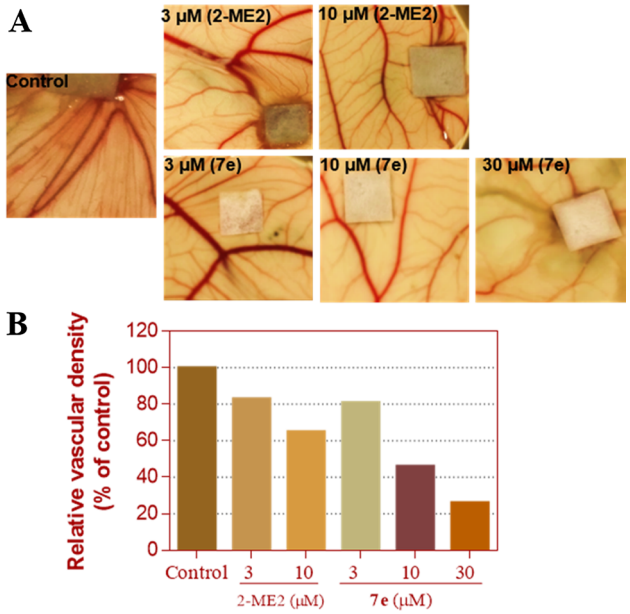

Fig. 10. *In vivo* inhibitory effects s of 7e on new blood formation or angiogenesis in the CAM assay. The photograph represents triplicate experiments. (B) The Semiquantitative scoring of CAM vessels was calculated and expressed as percentage vascular density relative to control.

synthesis of 3, 9-di-O-substituted coumestrol analogues **7a-7e** and their furan ring-opened analogs **5a-5e** through a modified DEC-mediated *in situ* lactonization strategy, and their anticancer efficacy on MCF-7, PC3, HepG2 and HCT116 human cancer cells.

In this proof-of-concept study, we were able to show that it is feasible to synthesize 3, 9-di-O-substituted coumestrols being able to address the proliferation stimulation effect related to parent coumestrol for the treatment of breast cancer. Our initial SAR studies revealed a preference for the furan ring-closed series and the small size basic group at 9-O position of coumestrol, especially the dimethylamine containing analogue **7e** which markedly inhibit the proliferation of MCF-7, PC3 and HepG2 cells and exhibited stronger effects than the parent coumestrol (1.7-fold increase), while lacking estrogenic activity (> 20 times weaker ERα binder). Further mechanism investigation revealed that **7e** was able to induce apoptosis, arrest cell cycle at G2/M phase and disrupt mitochondrial membrane potential in MCF7 cells via tubulin polymerization inhibition. In addition, **7e** significantly inhibit angiogenesis in a dose-dependent manner *in vivo*, which is consistent with the vascular disrupting effect induced by tubulin binding agents [53]. However, due to the overall moderate cell growth inhibition obtained here, more structure modifications on this lead compound **7e** towards potent anticancer agents are required in the future.

4. Experimental section

4.1. Chemistry

4.1.1. General

Reactions were monitored by thin-layer chromatography (TLC) using precoated silica gel plates (silica gel GF/UV 254), and spots were visualized under UV light (254 nm). Melting points (uncorrected) were determined on a Mel-TEMP II melting point apparatus and are uncorrected. Infrared (IR) spectra (KBr) were recorded on a Nicolet Impact 410 instrument (KBr pellet). ^{1}H NMR and ^{13}C NMR spectra were recorded with a Bruker Avance 300 MHz spectrometer at 300 K, using TMS as an internal standard. MS spectra were recorded on a Shimadzu GC-MS 2050 (ESI) or an Agilent 1946A-MSD (ESI) Mass Spectrum. Column chromatography was performed with silica gel (200–300 mesh). Chemical shifts (d) are expressed in parts per million relative to tetramethylsilane, which was used as an internal standard, coupling constants (J) are in hertz (Hz), and the signals are designated as follows: s, singlet; d, doublet; t, triplet; m, multiplet.

4.1.2. 1-(2,4-dihydroxyphenyl)-2-(4-methoxyphenyl)ethan-1-one (3)

Resorcinol (13.3 g, 120.6 mmol) and 4-methoxyphenylacetic (20.0 g, 120.6 mmol) were dissolved in BF_3-OEt_2 (360 mL) and heated at 80 °C for 3 h. The reaction mixture was cooled to room temperaturepoured, then poured into ice water (600 mL), extracted with ethyl acetate. The combined organic layer was washed with saturated $NaHCO_3$ solution and brine, dried over anhydrous Na_2SO_4, and concentrated under reduced pressure. The resulting compound was further purified by recrystallization (EtOH and EA). Off-white crystals; yield: 76%, Mp 150–152 °C; ^{1}H (300 MHz, DMSO) δ (ppm): 12.32 (s, 1H), 9.58 (s, 1H), 7.98 (d, J = 6.1 Hz, 1H), 7.34 (d, J = 6.3, 2H), 6.87 (d, J = 6.3, 2H), 6.56–6.43 (m, 2H), 4.23 (s, 2H), 3.97 (s, 3H). MS (ESI) m/z: 257.1 ([M–H]$^-$).

*4.1.3. 4,7-dihydroxy-3-(4-methoxyphenyl)-2H-chromen-2-one (**4**)*

To a solution of intermediate **3** (3.9 g, 15 mmol) in distilled 30 mL diethyl carbonate (DEC) and anhydrous toluene (30 mL) was added 3.6 g NaH (150 mmol) in batches at 0 °C with vigorous stirring. The temperature was slowly warmed to 120 °C and stirred for 3 h under N_2 atmosphere. The solvent was removed by rotary evaporator. Ice water was added slowly to the remaining mixture. The pH was carefully adjusted to 1–2 by adding 6 N HCl until the precipitate appeared which was further purified by recrystallization (Hexane and EA). White powder; yield: 75%, ^{1}H (300 MHz, DMSO) δ (ppm): 10.96 (s, 1H), 10.52 (s, 1H), 7.81 (d, *J* = 8.7 Hz, 1H), 7.29 (d, *J* = 8.6 Hz, 2H), 6.97 (d, *J* = 8.7 Hz, 2H), 6.80 (dd, *J* = 8.7, 2.2 Hz, 1H), 6.71 (d, *J* = 2.2 Hz, 1H), 3.79 (s, 3H), ESI-MS *m/z*: 283.1 ([M–H]$^-$).

*4.1.4. General procedure for the synthesis of target compounds (**5a-5e**)*

To a solution of intermediate **4** (0.2 g, 0.7 mmol) and corresponding 2-chloro-1-amine hydrochloride (2.1 mmol) in 2 mL anhydrous DMF was added anhydrous trisodium phosphate (1.14 g, 7.04 mmol). The reaction mixture was heated at 90 °C under N_2 atmosphere for 8–12 h, and then cooled to rt and poured into ice-cold water (15 mL) of which the pH was slowly adjusted to 6–7 by adding 0.5 N of hydrochloric acid. The mixture was then extracted with ethyl acetate. The organic phase was collected, dried with Na_2SO_4 and evaporated to get crude product which was then purified by column chromatograph to give final compounds **5a-5e**.

*4.1.5. 4-hydroxy-3-(4-methoxyphenyl)-7-(2-morpholinoethoxy)-2H-chromen-2-one (**5a**)*

Light red solid (50 mg); yield: 18%, Mp 187–191 °C. IR (KBr): 2923, 2859, 1713, 1609, 1577, 1103, 931 cm^{-1}. ^{1}H (300 MHz, DMSO) δ (ppm): 1H NMR (300 MHz, DMSO) *δ* 10.63 (s, 1H), 7.79 (d, *J* = 8.7 Hz, 1H), 7.33 (t, *J* = 7.0 Hz, 2H), 7.04–6.93 (m, 2H), 6.82 (dd, *J* = 8.7, 1.9 Hz, 1H), 6.74 (d, *J* = 1.9 Hz, 1H), 3.79 (s, 3H), 3.67 (t, *J* = 5.1 Hz, 4H), 3.38 (s, 4H), 2.45 (t, *J* = 5.2 Hz, 2H), 2.20 (s, 4H). MS (ESI) *m/z*: 398.1 ([M + H]$^+$), 420.1 ([M + K]$^+$). HRMS (ESI) *m/z* calcd. for $C_{22}H_{24}NO_6$ = 398.1598 [M + H]$^+$, found 398.1598.

*4.1.6. 4-hydroxy-3-(4-methoxyphenyl)-7-(2-(piperidin-1-yl)ethoxy)-2H-chromen-2-one (**5b**)*

Light red solid (92 mg); yield: 33%, Mp 157–159 °C. IR (KBr): 3446, 2933, 2853, 1718, 1604, 1512, 1247, 1129, 1038 cm^{-1}. ^{1}H (300 MHz, DMSO) δ (ppm): 10.68 (s, 1H), 7.78 (d, *J* = 8.4 Hz, 1H), 7.31 (t, *J* = 7.5 Hz, 2H), 6.98 (d, *J* = 8.4 Hz, 2H), 6.82 (d, *J* = 8.6 Hz, 1H), 6.76 (d, *J* = 6.2 Hz, 1H), 3.80 (s, 3H), 3.66 (t, *J* = 5.1 Hz, 4H), 2.54 (t, *J* = 5.2 Hz, 2H), 2.41(s, 4H), 1.56 (d, *J* = 5.2 Hz, 4H), 1.41–1.43 (m, 2H). MS (ESI) *m/z*: 394.1 ([M–H]$^-$). HRMS (ESI) *m/z* calcd. for $C_{23}H_{26}NO_5$ = 396.1805 [M + H]$^+$, found 396.1813.

*4.1.7. 4-hydroxy-3-(4-methoxyphenyl)-7-(2-(pyrrolidin-1-yl)ethoxy)-2H-chromen-2-one (**5c**)*

Light red solid (77 mg); yield: 29%, Mp 148–150 °C. IR (KBr): 3447, 2959, 2930, 1707, 1605, 1577, 1512, 1245, 1129, 831 cm^{-1}. ^{1}H (300 MHz, DMSO) δ (ppm): 10.87 (s, 1H), 7.74 (d, *J* = 8.4 Hz, 1H), 7.33 (d, *J* = 7.3 Hz, 2H), 6.99 (d, *J* = 7.5 Hz, 2H), 6.82 (d, *J* = 8.8 Hz, 1H), 6.73 (s, 1H), 3.80 (s, 3H), 3.66 (t, *J* = 5.6 Hz, 2H), 2.58 (t, *J* = 5.6 Hz, 2H), 2.31 (s, 4H), 1.58 (s, 4H). MS (ESI) *m/z*: 382.1 ([M + H]$^+$). HRMS (ESI) *m/z* calcd. for $C_{22}H_{24}NO_5$ = 382.1649 [M + H]$^+$, found 382.1648.

*4.1.8. 7-(2-(diethylamino)ethoxy)-4-hydroxy-3-(4-methoxyphenyl)-2H-chromen-2-one (**5d**)*

Light yellow solid (90 mg); yield: 33%, Mp 153–156 °C. IR (KBr): 3427, 2973, 1713, 1611, 1514, 1245, 1130, 846 cm^{-1}. ^{1}H (300 MHz, DMSO) δ (ppm): 10.72 (s, 1H), 7.76 (d, *J* = 8.8 Hz, 1H), 7.33 (d, *J* = 8.4 Hz, 2H), 7.00 (d, *J* = 8.4 Hz, 2H), 6.81 (d, *J* = 8.8 Hz, 1H), 6.75 (d, *J* = 7.2 Hz, 1H), 3.79 (s, 3H), 3.61 (t, *J* = 6.0 Hz, 2H), 2.56 (t, *J* = 6.0 Hz, 2H), 2.33 (dd, *J* = 13.9, 6.9 Hz, 4H), 0.81 (t, *J* = 7.0 Hz, 6H). MS (ESI) *m/z*: 384.1 ([M + H]$^+$). HRMS (ESI) *m/z* calcd. for $C_{22}H_{26}NO_5$ = 384.1805 [M + H]$^+$, found 384.1803.

*4.1.9. 7-(2-(dimethylamino)ethoxy)-4-hydroxy-3-(4-methoxyphenyl)-2H-chromen-2-one (**5e**)*

Light yellow solid (56 mg); yield: 22%, Mp 153–155 °C. IR (KBr): 3402, 2962, 2873, 1721, 1612, 1574, 1357, 1298, 1253, 1128, 829 cm^{-1}. ^{1}H (300 MHz, DMSO) δ (ppm): 10.74 (s, 1H), 7.75 (d, *J* = 8.6 Hz, 1H), 7.33 (d, *J* = 7.8 Hz, 2H), 6.98 (d, *J* = 8.0 Hz, 2H), 6.81 (d, *J* = 8.8 Hz, 1H), 6.74 (s, 1H), 3.81 (s, 3H), 3.64 (m, 2H), 2.56 (m, 2H), 2.28 (s, 6H). MS (ESI) *m/z*: 354.1 ([M–H]$^-$).

*4.1.10. 3-hydroxy-9-methoxy-6H-benzofuro[3,2-c]chromen-6-one (**6**)*

To a solution of substituted 4-hydroxy coumarin **4** (1.0 g, 3.5 mmol) in dried 1,2-dichloroethane (40 mL) was added ferric chloride/SiO_2 (50/50, w/w, 8.75 mmol) with stirring at reflux temperature under N_2 at atmosphere, and the reaction process was monitored by TLC analysis [42]. The reaction mixture was then evaporated under vacuum to remove the solvent. The residue was purified by silica gel chromatography to give the desired product. Gray solid (0.6 g), yield: 61%, Mp 98–101 °C; MS (ESI) *m/z*: 281.1 ([M − H]$^-$).

*4.1.11. General procedure for the synthesis of target compounds (**7a-7e**)*

To a solution of intermediate **6** (0.2 g, 0.7 mmol) and corresponding 2-chloro-1-amine hydrochloride (2.1 mmol) in 2 mL anhydrous THF was added anhydrous trisodium phosphate (1.14 g, 7.04 mmol). The reaction mixture was heated at 60 °C under N_2 atmosphere and the reaction process was monitored by TLC analysis. After completion, the reaction mixture was then evaporated under vacuum to remove the solvent, then the residue was dissolved in water (15 mL) and extracted with ethyl acetate. The organic phase was collected, dried with Na_2SO_4 and evaporated to get crude product which was then purified by column chromatograph to give final compounds **7a-7e**.

*4.1.12. 9-methoxy-3-(2-morpholinoethoxy)-6H-benzofuro[3,2-c]chromen-6-one (**7a**)*

Pale white solid (150 mg); yield: 54%, Mp > 300 °C. IR (KBr): 2924, 2852, 1746, 1629, 1258, 1115, 825 cm^{-1}. ^{1}H (300 MHz, $CDCl_3$) δ (ppm): 7.97 (d, *J* = 8.6 Hz, 2H), 7.88 (d, *J* = 9.4 Hz, 1H), 7.18 (d, *J* = 1.9 Hz, 1H), 7.06 (dd, *J* = 8.6, 2.1 Hz, 1H), 7.02–6.93 (m, 2H), 4.22 (t, *J* = 5.5 Hz, 2H), 3.93 (s, 3H), 3.81–3.73 (m, 4H), 2.89 (t, *J* = 5.5 Hz, 2H), 2.64 (d, *J* = 4.3 Hz, 4H). MS (ESI) *m/z*: 396.1 ([M + H]$^+$), 418.2 ([M + Na]$^+$). HRMS (ESI) *m/z* calcd. for $C_{22}H_{22}NO_6$ = 396.1442 [M + H]$^+$, found 396.1444.

*4.1.13. 9-methoxy-3-(2-(piperidin-1-yl)ethoxy)-6H-benzofuro[3,2-c]chromen-6-one (**7b**)*

Pale white solid (210 mg); yield: 75%, Mp > 300 °C. IR (KBr): 2924, 2853, 1748, 1629, 1439, 1258, 811 cm^{-1}; ^{1}H NMR (300 MHz, $CDCl_3$): δ (ppm): 7.95 (dd, *J* = 8.6, 3.7 Hz, 1H), 7.90–7.83 (m, 1H), 7.16 (t, *J* = 3.6 Hz, 1H), 7.05 (dd, *J* = 8.6, 2.2 Hz, 1H), 7.00 (dd, *J* = 4.5, 2.3 Hz, 2H), 4.21 (t, *J* = 5.9 Hz, 2H), 3.92 (s, 3H), 2.85 (t, *J* = 5.9 Hz, 2H), 2.56 (s, 4H), 1.65 (dt, *J* = 10.9, 5.6 Hz, 4H), 1.52–1.44 (m, 2H). ^{13}C NMR (75 MHz, $CDCl_3$) *δ* 161.2, 159.3, 158.6, 157.8, 155.8, 154.3, 121.74, 120.9, 115.9, 112.7, 112.6, 105.4, 101.4, 96.1, 66.1, 57.1, 55.3, 54.6, 25.4, 23.6. MS (ESI) *m/z*: 394.1 ([M + H]$^+$). HRMS (ESI) *m/z* calcd. for $C_{23}H_{24}NO_5$ = 394.1649 [M + H]$^+$, found 394.1655.

*4.1.14. 9-methoxy-3-(2-(pyrrolidin-1-yl)ethoxy)-6H-benzofuro[3,2-c]chromen-6-one (**7c**)*

Pale white solid (180 mg); yield: 61%, Mp > 300 °C. IR (KBr): 2962, 2919, 1735, 1631, 1258, 1101, 805 cm^{-1}; ^{1}H NMR (300 MHz, $CDCl_3$): δ (ppm): 7.97 (d, *J* = 8.6 Hz, 1H), 7.89 (d, *J* = 9.4 Hz, 1H), 7.19 (d, *J* = 2.0 Hz, 1H), 7.06 (dd, *J* = 14.2, 5.6 Hz, 3H), 4.24 (t, *J* = 5.7 Hz, 2H), 3.93 (s, 3H), 3.02 (t, *J* = 5.7 Hz, 2H), 2.72 (s, 4H),

1.87 (s, 4H). MS (ESI) *m/z*: 380.1 ($[M+H]^+$). HRMS (ESI) *m/z* calcd. for $C_{22}H_{22}NO_5$ = 380.1494 $[M+H]^+$, found 380.1494.

4.1.15. 3-(2-(diethylamino)ethoxy)-9-methoxy-6H-benzofuro[3,2-c] chromen-6-one (7d)

Light yellow solid (230 mg); yield: 85%, Mp > 300 °C. IR (KBr): 2961, 2924, 1734, 1631, 1497, 1259, 1103, 801 cm^{-1}; ^1H NMR (300 MHz, $CDCl_3$): δ (ppm): 7.94 (d, *J* = 8.6 Hz, 1H), 7.85 (d, *J* = 9.3 Hz, 1H), 7.16 (d, *J* = 2.1 Hz, 1H), 7.04 (dd, *J* = 8.6, 2.2 Hz, 1H), 7.00–6.96 (m, 2H), 4.15 (t, *J* = 6.0 Hz, 2H), 3.92 (s, 3H), 2.96 (t, *J* = 6.0 Hz, 2H), 2.69 (t, *J* = 7.1 Hz, 4H), 1.12 (t, *J* = 7.2 Hz, 6H). MS (ESI) *m/z*: 382.1 ($[M+H]^+$). HRMS (ESI) *m/z* calcd. for $C_{22}H_{24}NO_5$ = 382.1649 $[M+H]^+$, found 382.1652.

4.1.16. 3-(2-(dimethylamino)ethoxy)-9-methoxy-6H-benzofuro[3,2-c] chromen-6-one (7e)

Pale white solid (240 mg); yield: 64%, Mp > 300 °C. IR (KBr): 2933, 2834, 1741, 1632, 1531, 1257, 1099, 840 cm^{-1}; ^1H NMR (300 MHz, $CDCl_3$): δ (ppm): 7.96 (d, *J* = 8.6 Hz, 1H), 7.88 (d, *J* = 8.9 Hz, 1H), 7.18 (d, *J* = 2.0 Hz, 1H), 7.10–6.95 (m, 3H), 4.17 (t, *J* = 5.5 Hz, 2H), 3.92 (s, 3H), 2.81 (t, *J* = 5.5 Hz, 2H), 2.39 (s, 6H). MS (ESI) *m/z*: 354.1 ($[M+H]^+$). HRMS (ESI) *m/z* calcd. for $C_{20}H_{20}NO_5$ = 354.1336 $[M+H]^+$, found 354.1342.

4.2. Biological evaluation

4.2.1. MTT assay for anti-proliferative activities

Cells were cultured in RPMI1640 medium (containing 10% (v/v) FBS, 100 U/mL Penicillin and 100 mg/mL Streptomycin) in a 5% CO_2-humidified atmosphere at 37 °C. Cells were trypsinized and seeded at a density of 1×10^5/mL into a 96-well plate (100 mL/well) and incubated at 37 °C, 5% CO_2 atmosphere for 24 h. After this time they were treated with 100 mL/well medium containing all the test compounds which had been pre-prepared to provide the concentration range of 1.6×10^{-4} mol/L, 8×10^{-5} mol/L, 2×10^{-5} mol/L and 2×10^{-6} mol/L, and re-incubated for a further 72 h. Control wells were added the equivalent volume of medium containing 1% (v/v) DMSO. 20 μL MTT (5 mg/mL) was added and cells continued to incubate in darkness at 37 °C for 4 h. The culture medium was then removed carefully and 150 mL DMSO was added. The cells were maintained at room temperature in darkness for 20 min to ensure thorough color diffusion before reading the absorbance. The absorbance values were read at 490 nm for determination of IC_{50} values. To test the estrogenic activity of **7e**, MCF-7 cells were further treated with 100 mL/well medium containing **7e** which had been pre-prepared to provide the concentration range of 2×10^{-6} mol/L, 2×10^{-7} mol/L and 2×10^{-8} mol/L, and re-incubated for a further 72 h.

4.2.2. ERα binding affinity assay

The recombinant ERα (Thermo Fisher Scientific Inc., Invitrogen, USA) and the fluorescent estrogen ligands (self-made) were removed from the −80 °C freezer and thawed on ice for 1 h prior to use. The fluorescent estrogen ligand was added to the ERα and screening buffer (ES2 Screening Buffer, Invitrogen, USA) was added to make the final concentration 9 nM for fluorescent estrogen and 30 nM for ERα. Test compounds were accurately weighed and dissolved in DMSO, screening buffer was added to dilute to required concentration. Test compound (1 μL) was added to 49 μL screening buffer in each well (384-well microplate, Corning, USA). To this 50 μL of the fluorescent estrogen/ER complex was added to make up a final volume of 100 μL. A positive control contained 50 μL estradiol buffer (1 nM) and 50 μL fluorescent estrogen/ER complexes. A negative control contained 50 μL screening buffer and 50 μL fluorescent estrogen/ER complexes. The negative control was used to determine the polarization value when no competitor was present (theoretical maximum polarization). The microplate was incubated in the dark at room temperature for 2 h and shaken on a plate shaker. The polarization values were read on a Safire microplate reader. Δ mP = Maximum mP- Minimum mP.

4.2.3. Cellular apoptosis study

Annexin V/PI staining assay was used to assess the mechanism of cell death. MCF-7 cells were treated without or with **7e** (10, 15 and 20 μM) for 24 h. Then, cells were collected, washed with PBS, and stained with 5 μL annexin V fluorescein isothiocyanate (FITC) for 15 min at RT, then 5 μL PI for 5 min at RT. After that, the samples were analyzed by flow cytometry using FACScalibur (Becton Dickinson). The cell distributions were calculated using Cell Quest software (Becton Dickinson).

4.2.4. Cell cycle analysis

MCF-7 cells were seeded on 6-well plates and treated with 10 μM, 15 μM, 20 μM of **7e** for 24 h. After treatment, the cells were washed twice with ice-cold PBS, collected by centrifugation, and fixed in ice-cold 70% (v/v) ethanol, washed with PBS, re-suspended with 0.1 mg/mL RNase, stained with 40 mg/mL PI, and analyzed by flow cytometry using FACScalibur (Becton Dickinson). The cell cycle distributions were calculated using Cell Quest software (Becton Dickinson).

4.2.5. Mitochondrial membrane potential assay

The level of MMP in the cells was monitored using a lipophilic cationic fluorescent probe 5, 50, 6, 60-tetrachloro-1,10,3,30-tetraethylbenzimidaolylcarbocyanine iodide JC-1 (Beyotime, China), which appears as aggregates and emits red fluorescence in the presence of high MMP. When MMP reduces in apoptotic cells, JC-1 displays as monomers indicated by green fluorescence. MCF-7 cells were seeded on 6-well plates and treated with 10 μM, 15 μM, 20 μM of **7e** for 24 h. JC-1 Compensation for Flow Cytometry was carried out as follows, untreated healthy cells as the negative control and CCCP (10 μM)-treated cells as the positive control. After treatment, the cells were washed twice with ice-cold PBS, collected by centrifugation, and re-suspended with 0.5 mL RPMI1640 medium, Then, the cells were harvested by centrifugation and incubated with JC-1 solution for 30 min. After briefly washing, the proportion of green and red fluorescence intensity were immediately detected and analyzed by flow cytometry using FACScalibur (Becton Dickinson).

4.2.6. Western blots

MCF-7 cells were seeded on 6-well plates and incubated for 24 h in the presence or absence of the test compounds **7e** (10 and 15 μM). Then cells were washed twice with PBS, then collected and lysed in lysis buffer (100 mM of Tris-Cl, pH 6.8, 4% (m/v) SDS, 20% (v/v) glycerol, 200 mM of β-mercaptoethanol, 1 mM of PMSF, 0.1 mM NaF and DTT) for 1 h on the ice. The lysates were then subjected to centrifugation (14,000 rpm) at 4 °C for 5 min. Protein concentration in the supernatants was detected by BCA protein assay (Thermo, Waltham, MA). Then equal amount of protein was separated with 12% SDS-PAGE and transferred to polyvinylidene difluoride (PVDF) membranes (Millipore, Bedford, MA) using a semi-dry transfer system (Bio-rad, Hercules, CA). Proteins were detected using specific antibodies overnight at 4 °C followed by HRP-conjugated secondary antibodies for 1 h at 37 °C. All of the antibodies were diluted in PBST containing 1% BSA. Enhanced chemiluminescent reagents (Beyotime, Jiangsu, China) were used to detect the HRP on the immunoblots, and the visualized bands were captured by film. The bands were quantified by Quantity One software (Vision 4.62, Bio-rad, Hercules, CA), and the relative protein level were normalized to β-actin.

4.2.7. In vitro tubulin polymerization inhibition

Porcine microtubules were purified from porcine brain using two cycles of polymerization-depolymerization in a high-molarity buffer as described previously [56]. Protein concentration in the supernatants was detected by BCA protein assay (Thermo, Waltham, MA).

Subsequently, 0.6 mg/mL purified tubulin, 1 M glutamate and 1 mM GTP were mixed in RB buffer (100 mM MES (Ph 6.8), 1 mM EGTA, 0.5 mM MgCl2). One of the tested compounds was then added and incubated for 10 min on ice. Samples were transferred into cuvette and tubulin polymerization was determined by monitoring the absorbance at 350 nm at 37 °C using a thermostatic spectrophotometer (Beckman Coulter). Final tubulin polymerization rate (control %) at 24 min was monitored by increase in the fluorescence mentioned above at 37 °C.

4.2.8. Immunohistochemistry

MCF-7 cells were seeded on glass cover slips and incubated for 24 h in the presence or absence of the test compounds **7e** (15 μM) and colchicine (1 μM). After treatment, the cover slips were fixed with a 4% paraformaldehyde solution for 15 min at room temperature and washed twice with PBS. Cell permeabilization was achieved by administration of a 2% Triton X-100 solution for 15 min. The cover slips were blocked with a 1% bovine serum albumin (BSA) solution for 30 min and then incubated with anti-α-tubulin antibody at 4 °C overnight. The slides were washed three times for 5 min each with PBS. Next, the cover slips were incubated with FITC-conjugated anti-mouse secondary antibody at room temperature for 30 min and then washed three times with PBS solution. Finally, the cells were observed under a fluorescence microscope, and the pictures were analyzed for the integrity of the microtubule network.

4.2.9. Chicken chorioallantoic membrane (CAM) assay

Fertilized eggs were incubated for 7 days in a humidified environment at 37 °C with 5% CO_2 in air and saturated humidity. Then, a window of approximately 1 cm_2 was opened on the egg shell to expose the CAM. Test compound **7e** (3, 10 and 30 μM) and positive control 2-ME2 (3 and 10 μM) dissolved in DMSO were placed on sterile methyl cellulose filter papers with phosphate buffered saline as the blank control. The papers were then placed on the CAM. The window was sealed with sterile cellophane tape. The eggs were further incubated at 37 °C under a constant relative humidity of 60% for 72 h. After fixed with acetone and ethanol for 10 min, the CAM was cut, and papers removed to observe angiogenesis. Images of the control and sample-treated areas were captured.

4.2.10. Molecular modeling

The molecular modeling was performed with Discovery Studio.3.0/CDOCK protocol (Accelrys Software Inc.). The crystal structures of ERα complexed with 2-ME2 (PDB code: 3UUD) were downloaded from Protein Data Bank. Coumestrol was drowned and optimized using Hyperchem v7.0. The protein and ligand were optimized and charged with CHARMm force field to perform docking. Up to 10 conformations were retained, and binding modes presented graphically are representative of the highest-scored conformations.

4.2.11. Statistical analysis

The results are presented as the means ± SD, n = 3. Statistical analyses were conducted using the Graph Pad Prism software version 6 (San Diego California USA). One way ANNOVA followed by Dunnett's multiple comparison tests were used to identify statistical significance and p-values less than 0.05 ($p < 0.05$) were considered to be statistically significant.

Conflicts of interest

The authors declare no competing financial interest.

Acknowledgements

We thank China Pharmaceutical University for support.

Appendix A. Supplementary material

Supplementary data to this article can be found online at https://doi.org/10.1016/j.bioorg.2018.12.024.

References

[1] M. Pascolutti, R.J. Quinn, Natural products as lead structures: chemical transformations to create lead-like libraries, Drug Discov Today 19 (2014) 215–221.
[2] D.J. Newman, G.M. Cragg, Natural products as sources of new drugs over the 30 years from to 2010, J. Nat. Prod. 75 (2012) (1981) 311–335.
[3] A.L. Demain, P. Vaishnav, Natural products for cancer chemotherapy, Microb. Biotechnol. 4 (2011) 687–699.
[4] G.S. Luo, M.Q. Chen, W.T. Lyu, R.H. Zhao, Q. Xu, Q.D. You, H. Xiang, Design, synthesis, biological evaluation and molecular docking studies of novel 3-aryl-4-anilino-2H-chromen-2-one derivatives targeting ERα as anti-breast cancer agents, Bioorg. Med. Chem. Lett. 27 (2017) 2668–2673.
[5] G.S. Luo, X.Y. Li, G.Q. Zhang, C.Z. Wu, Z.P. Tang, L.Y. Liu, Q.D. You, H. Xiang, Novel SERMs based on 3-aryl-4-aryloxy-2H-chromen-2-one skeleton - a possible way to dual ERα/VEGFR-2 ligands for treatment of breast cancer, Eur. J. Med. Chem. 140 (2017) 252–273.
[6] F.G. Medina, J.G. Marrero, M. Macías-Alonso, M.C. González, I. Córdova-Guerrero, A.G. Teissier García, S. Osegueda-Robles, Coumarin heterocyclic derivatives: chemical synthesis and biological activity, Nat. Prod. Rep. 32 (2015) 1472–1507.
[7] W. Wang, Y.Y. Zhao, H. Liang, Q. Jia, H.B. Chen, Coumestans from Hedysarum multijugum, J. Nat. Prod. 69 (2006) 876–880.
[8] G.L. Xi, Z.Q. Liu, Coumestan inhibits radical-induced oxidation of DNA: is hydroxyl a necessary functional group, J. Agric. Food Chem. 62 (2014) 5636–5642.
[9] W. Zhang, S.C. Lun, S.H. Wang, X.W. Jiang, F. Yang, J. Tang, A.L. Manson, A.M. Earl, H. Gunosewoyo, W.R. Bishai, L.F. Yu, Identification of novel coumestan derivatives as polyketide synthase 13 inhibitors against mycobacterium tuberculosis, J. Med. Chem. 61 (2018) 791–803.
[10] T. Qwebani-Ogunleye, N.I. Kolesnikova, P. Steenkamp, C.B. de Koning, D. Brady, K.W. Wellington, A one-pot laccase-catalysed synthesis of coumestan derivatives and their anticancer activity, Bioorg. Med. Chem. 25 (2017) 1172–1182.
[11] E.M. Bickoff, A.N. Booth, R.L. Lyman, A.L. Livingston, C.R. Thompson, F. Deeds, Coumestrol, a new estrogen isolated from forage crops, Science 126 (1957) 969–970.
[12] International Diabetes Federation IDF Diabetes Atlas, sixth ed., International Diabetes Federation, Brussels, Belgium, 2013.
[13] A.H. Wu, M.C. Yu, C.C. Tseng, M.C. Pike, Epidemiology of soy exposures and breast cancer risk, Br. J. Cancer 98 (2008) 9–14.
[14] C. Nagata, T. Mizoue, K. Tanaka, I. Tsuji, A. Tamakoshi, K. Matsuo, et al., Soy intake and breast cancer risk: an evaluation based on a systematic review of epidemiologic evidence among the Japanese population, Jpn. J. Clin. Oncol. 44 (2014) 282–295.
[15] B.J. Trock, L. Hilakivi-Clarke, R. Clarke, Meta-analysis of soy intake and breast cancer risk, J. Natl. Cancer Inst. 98 (2006) 459–471.
[16] S.A. Lee, X.O. Shu, H. Li, G. Yang, H. Cai, W. Wen, et al., Adolescent and adult soy food intake and breast cancer risk: results from the Shanghai Women's Health Study, Am. J. Clin. Nutr. 89 (2009) 1920–1926.
[17] S.M. Mense, T.K. Hei, R.K. Ganju, H.K. Bhat, Phytoestrogens and breast cancer prevention: possible mechanisms of action, Environ. Health Perspect. 116 (2008) 426–433.
[18] M.G. Glazier, M.A. Bowman, A review of the evidence for the use of phytoestrogens as a replacement for traditional estrogen replacement therapy, Arch. Intern. Med. 161 (2001) 1161–1172.
[19] M. Messina, W. McCaskill-Stevens, J.W. Lampe, Addressing the soy and breast cancer relationship: review, commentary, and workshop proceedings, J. Natl. Cancer Inst. 98 (2006) 1275–1284.
[20] I.E. Obiorah, P. Fan, V.C. Jordan, Breast cancer cell apoptosis with phytoestrogens is dependent on an estrogen-deprived state, Cancer Prevention Res. 7 (2014) 939–949.
[21] S.Y. Cho, S. Cho, E. Park, B. Kim, E.J. Sohn, B. Oh, E.O. Lee, H.J. Lee, S.H. Kim, Coumestrol suppresses hypoxia inducible factor 1alpha by inhibiting ROS mediated sphingosine kinase 1 in hypoxic PC-3 prostate cancer cells, Bioorg. Med. Chem. Lett. 24 (2014) 2560–2564.
[22] J.H. Mitchell, S.J. Duthie, A.R. Collins, Effects of phytoestrogens on growth and DNA integrity in human prostate tumor cell lines: PC-3 and LNCaP, Nutr. Cancer 38 (2000) 223–228.
[23] E. Zhao, Q. Mu, Phytoestrogen biological actions on mammalian reproductive system and cancer growth, Sci. Pharm. 79 (2011) 1–20.
[24] Y.H. Lee, H.J. Yuk, K.H. Park, Y.S. Bae, Coumestrol induces senescence through protein kinase CKII inhibition-mediated reactive oxygen species production in human breast cancer and colon cancer cells, Food Chem. 141 (2013) 381–388.
[25] P. Diel, S. Olff, S. Schmidt, H. Michna, Effects of the environmental estrogens bisphenol A, o, p'-DDT, p-tert-octylphenol and coumestrol on apoptosis induction, cell proliferation and the expression of estrogen sensitive molecular parameters in the human breast cancer cell line MCF-7, J. Steroid. Biochem. Mol. Biol. 80 (2002) 61–70.
[26] A. Zafar, S. Singh, I. Naseem, Cytotoxic activity of soy phytoestrogen coumestrol against human breast cancer MCF-7 cells: insights into the molecular mechanism, Food Chem. Toxicol. 99 (2017) 149–161.
[27] A. Zafar, S. Singh, I. Naseem, Cu(II)-coumestrol interaction leads to ROS-mediated DNA damage and cell death: a putative mechanism for anticancer activity, J. Nutr.

Biochem. 33 (2016) 15–27.
[28] A. Zafar, S. Singh, Y.K. Satija, D. Saluja, I. Naseem, Deciphering the molecular mechanism underlying anticancer activity of coumestrol in triple-negative breast cancer cells, Toxicol In Vitro. 46 (2018) 19–28.
[29] W. Lim, M. Jeong, F.W. Bazer, G. Song, Coumestrol inhibits proliferation and migration of prostate cancer cells by regulating AKT, ERK1/2 and JNK MAPK cell signaling cascades, J. Cell Physiol. 232 (2017) 862–871.
[30] P.Y. Maximov, J.S. Lewis-Wambi, V.C. Jordan, The paradox of oestradiol-induced breast cancer cell growth and apoptosis, Curr. Signal Transduct. Ther. 4 (2009) 88–102.
[31] C. Dees, J.S. Foster, S. Ahamed, J. Wimalasena, Dietary estrogens stimulate human breast cells to enter the cell cycle, Environ. Health Presp. 105 (Suppl 3) (1997) 633–636.
[32] J.C. Nwachukwu, S. Srinivasan, N.E. Bruno, J. Nowak, N.J. Wright, F. Minutolo, E.S. Rangarajan, T. Izard, X.Q. Yao, B.J. Grant, D.J. Kojetin, O. Elemento, J.A. Katzenellenbogen, K.W. Nettles, Systems structural biology analysis of ligand effects on ERα predicts cellular response to environmental estrogens and anti-hormone therapies, Cell Chem. Biol. 24 (2017) 35–45.
[33] C. Chandsawangbhuwana, M.E. Baker, 3D models of human ERa and ERb complexed with coumestrol, Steroids 80 (2014) 37–43.
[34] V. Delfosse, M. Grimaldi, J.L. Pons, A. Boulahtouf, A. le Maire, V. Cavailles, G. Labesse, W. Bourguet, P. Balaguer, Structural and mechanistic insights into bisphenols action provide guidelines for risk assessment and discovery of bisphenol A substitutes, Proc. Natl. Acad. Sci. USA 109 (2012) 14930–14935.
[35] B.L. Bergquist, K.G. Jefferson, H.N. Kintz, A.E. Barber, A.A. Yeagley, Disconnecting the estrogen receptor binding properties and antimicrobial properties of parabens through 3,5-substitution, ACS Med. Chem. Lett. 9 (2017) 51–55.
[36] V.C. Jordan, The new biology of estrogen-induced apoptosis applied to treat and prevent breast cancer, Endocr. Relat. Cancer. 22 (2015) R1–R31.
[37] T. Yao, D. Yue, R.C. Larock, An efficient synthesis of coumestrol and coumestans by iodocyclization and Pd-catalyzed intramolecular lactonization, J. Org. Chem. 70 (2005) 9985–9989.
[38] C.C. Li, Z.X. Xie, Y.D. Zhang, J.H. Chen, Z. Yang, Total synthesis of wedelolactone, J. Org. Chem. 68 (2003) 8500–8504.
[39] U.A. Kshirsagar, R. Parnes, H. Goldshtein, R. Ofir, R. Zarivach, D. Pappo, Aerobic iron-based cross-dehydrogenative coupling enables efficient diversity-oriented synthesis of coumestrol-based selective estrogen receptor modulators, Chemistry 19 (2013) 13575–13583.
[40] J. Zhang, J. Qiu, C. Xiao, L. Yu, F. Yang, J. Tang, Metal-free tandem oxidative coupling of primary alcohols with azoles for the synthesis of hemiaminal ethers, Eur. J. Org. Chem. 81 (2016) 3380–3385.
[41] J.F. Sheng, T.L. Xu, E.S. Zhang, X.J. Zhang, W.T. Wei, Y. Zou, Synthesis of coumestrol and aureol, J. Nat. Prod. 79 (2016) 2749–2753.
[42] L.N. Tang, Y.L. Pang, Q. Yan, L.Q. Shi, J.H. Huang, Y.F. Du, K. Zhao, Synthesis of coumestan derivatives via $FeCl_3$-mediated oxidative ring closure of 4-hydroxy coumarins, J. Org. Chem. 76 (2011) 2744–2752.
[43] X. Hu, R.W. Jiao, H.N. Li, X.H. Wang, H.D. Lyu, X. Gao, F.X. Xu, Z.L. Li, H.M. Hua, D.H. Li, Antiproliferative hydrogen sulfide releasing evodiamine derivatives and their apoptosis inducing properties, Eur. J. Med. Chem. 151 (2018) 376–388.
[44] C. Wang, M.S. Kurzer, Phytoestrogen concentration determines effects on DNA synthesis in human breast cancer cells, Nutr. Cancer 28 (1997) 236–247.
[45] Y. Mousavi, H. Adlercreutz, Enterolactone and estradiol inhibit each other's proliferative effect on MCF-7 breast cancer cells in culture, J. Steroid Biochem. Mol. Biol 14 (1992) 615–619.
[46] S. Lecomte, M. Lelong, G. Bourgine, T. Efstathiou, C. Saligaut, F. Pakdel, Assessment of the potential activity of major dietary compounds asselective estrogen receptor modulators in two distinct cell models forproliferation and differentiation, Toxicol. Appl. Pharmacol. 325 (2017) 61–70.
[47] K.T. Chan, F.Y. Meng, Q. Li, C.Y. Ho, T.S. Lam, Y. To, W.H. Lee, M. Li, K.H. Chu, M. Toh, Cucurbitacin B induces apoptosis and S phase cell cycle arrest in BEL-7402 huma hepatocellular carcinoma cells and is effective via oral administration, Cancer Lett. 294 (2010) 24–118.
[48] C.X. Wang, R.J. Youle, The role of mitochondria in apoptosis, Ann. Rev. Genet. 43 (2009) 95–118.
[49] M. Jackman, C. Lindon, E.A. Nigg, J. Pines, Active cyclin B1-Cdk1 first appears on centrosomes in prophase, Nat. Cell Biol. 5 (2003) 143–148.
[50] A.B. Edsall, A.K. Mohanakrishnan, D. Yang, P.E. Fanwick, E. Hamel, A.D. Hanson, G.E. Agoston, M. Cushman, Effects of altering the electronics of 2-methoxyestradiol on cell proliferation, on cytotoxicity in human cancer cell cultures, and on tubulin polymerization, J. Med. Chem. 47 (2004) 5126–5139.
[51] A. Alsayari, L. Kopel, M.S. Ahmed, A. Pay, T. Carlson, F.T. Halaweish, Design, synthesis, and biological evaluation of steroidal analogs as estrogenic/anti-estrogenic agents, Steroids 118 (2017) 32–40.
[52] P.R. Clarke, L.A. Allan, Cell-cycle control in the face of damage-a matter of life or death, Trends Cell Biol. 19 (2009) 89–98.
[53] G.G. Dark, S.A. Hill, V.E. Prise, G.M. Tozer, G.R. Pettit, D.J. Chaplin, Combretastatin A-4, an agent that displays potent and selective toxicity toward tumor vasculature, Cancer Res. 57 (1997) 1829–1834.
[54] W. Chen, G.X. Zhang, L. Guo, W.X. Fan, Q. Ma, X.D. Zhang, R.L. Du, R.H. Cao, Synthesis and biological evaluation of novel alkyl diamine linked bivalent b-carbolines as angiogenesis inhibitors, Eur. J. Med. Chem. 124 (2016) 249–261.
[55] M. Chen, Y. Rao, Y. Zheng, S. Wei, Y. Li, T. Guo, et al., Association between soy isoflavone intake and breast cancer risk for pre- and post-menopausal women: a meta-analysis of epidemiological studies, PLoS ONE 9 (2014) e89288.
[56] M. Castoldi, A.V. Popov, Purification of brain tubulin through two cycles of polymerization-depolymerization in a high-molarity buffer, Protein Expr. Purif. 32 (2003) 83–88.